Hindawi
Journal of Sensors
Volume 2022, Article ID 9376885, 11 pages
https://doi.org/10.1155/2022/9376885

Research Article

A Method Applied in Anomaly Detection of Impurities Adhering to Pipes of Coriolis Mass Flowmeter

Jianxin Ren,[1] **Yixin Qin**,[1] **Peng Yang**,[1] **and Peng Zhang**[2]

[1]*School of Automation, Northwestern Polytechnical University, Xi'an, China*
[2]*Xi'an Dongfeng Electrical Co., Ltd., Xi'an, China*

Correspondence should be addressed to Jianxin Ren; renjianxin@nwpu.edu.cn

Received 24 September 2021; Revised 26 May 2022; Accepted 27 May 2022; Published 15 June 2022

Academic Editor: Akhilesh Pathak

The Coriolis mass flowmeter (CMF) is widely used to measure mass flow, mainly in petrochemical, medical, pharmaceutical, food manufacturing, and other industries. The measuring tube is the crucial component of CMF, which affects the measurement accuracy and causes losses to the production of enterprises. Wall-mounted failure of the measuring tube affects measurement accuracy. A real-time detection method based on acceleration sensor array signal processing and pattern recognition are proposed to detect such failure. Two acceleration sensors are arranged outside the CMF to compose a five-channel sensor array. The signals of the multichannel array are decomposed through a blind source separation algorithm, and array signal features are extracted by a wavelet scattering network. Support vector data description (SVDD) is used to detect the hanging state of CMF at last. The experimental results show that the proposed method can be used to detect the CMF wall-mounted failure in real-time with an accuracy of 89.59%, and the method can reduce production losses.

1. Introduction

Coriolis mass flowmeter (CMF) is an instrument that can directly measure the mass flow of fluid without intermediate parameter conversion [1]. Compared with other traditional instruments for measuring mass flow, CMF has significant advantages such as high measurement accuracy, no moving parts, long service life, and slight wear. CMF has been widely used in fluid detection in petrochemical, food, medical, pharmaceutical, and other fields [2]. A typical CMF consists of measuring tubes, drive units, and sensors [3]. The quality of the impurities attached to the measuring tube greatly influences the measurement accuracy of the CMF. The higher the vibration frequency of the CMF, the greater the impact of the attached impurities on the measurement accuracy [4]. Due to long-term operation, the impurities in the fluid are deposited in the measuring tube leading to unbalance in the measuring tube. It affects the calibration factor of the flowmeter and the flow phase calculation of the CMF [5]. Vibration signal detection and analysis is a common method to detect the impurities in the CMF measuring tube. X-ray and ultrasonic imaging technology are often used to inspect the interior of the CMF measuring tube. However, these methods are either expensive or need additional equipment on the measuring tube, making it difficult to meet the requirements of real-time detection of impurity adhesion of CMF measuring tube [6, 7]. Since the acceleration sensor can accurately detect the acceleration changes and convert them into usable output signals, it can be mounted on the CMF baffle to evaluate the quality of impurities attached to the CMF measuring tube without installing any equipment.

The signal collected from the CMF measuring tube by the acceleration sensor array is a large amount of data. The machine learning algorithm is a good data analysis and quality evaluation solution for such mass data problems. There are many methods for fault detection of CMF. Stark et al. proposed a multimode method to detect the fault state of CMF and completed the design of corresponding diagnostic equipment [8]. Yang et al. proposed an algorithm for CMF fault detection and correction based on threshold comparison [9]. This method improved the measurement accuracy

without increasing the system cost by adding corresponding algorithms to the existing software. Gao et al. realized feature recognition and correction of results by the neural networks [10]. Sun and Wang discussed and compared two verification methods of CMF: online verification and offline verification [11]. Wheeler et al. proposed a method to detect the faults of CMF through the change of its stiffness. However, this method can only be carried out when CMF is not working [12]. Array signal processing consists of array signal decomposition, signal feature extraction, and abnormal signal detection. Wang et al. proposed a bearing fault diagnosis method based on the combination of the fast independent component analysis (FastICA) in blind source separation and envelope spectrum analysis to identify the bearing fault signal characteristics under complex paths [13]. Multichannel data acquisition signals are mixed signals of the original signal. The FastICA preprocess them to obtain the source signal, which is a fast optimization iterative algorithm applicable to any type of data [14]. The effect of the machine learning detection algorithm depends on the extraction of signal features. There are many methods to extract signal features, such as empirical mode decomposition (EMD), Fourier transform, and wavelet transform [15]. EMD has problems with mode aliasing and endpoint effect, Fourier transform cannot be used for nonstationary signals, and wavelet transform has a wider range of applications to signals and retains time information [16–18]. An invariant scattering convolution network is a good feature extraction method based on wavelet transform. The one-class classification algorithm based on support vector data description (SVDD) is adopted in abnormal signal detection. The basic idea of the algorithm is to establish an optimal hypersphere for the data and then determine whether the sample is in the hypersphere for classification [19]. The array signal is decomposed by FastICA, and the original signal is obtained in this paper. The original signal's characteristics are extracted using the wavelet scattering network to train the SVDD anomaly detection model and realize outlier detection of the CMF.

This paper aims to present a CMF wall-mounted failure detection system without additional equipment on the measuring tube. The CMF measurement tube wall-mounted failure can be detected by analyzing the array signal. The principles and methodology are introduced in Section 2. Simulations and experiments are analyzed in Section 3. Some reasonable explanations of simulation results and experimental data are given in the last.

2. Principles and Methodology

2.1. Working Principle of CMF. CMF consists of a primary instrument and a secondary instrument, as shown in Figure 1(a). The primary instrument includes the flange, shunt body, measuring tube (U-shape), drive unit, and detection units, as shown in Figure 1(b). The secondary instrument is a transmitter that processes the output signal of the primary instrument.

The flange is used to connect the measuring tube and the secondary instrument. The shunt body is used to evenly divide the measured liquid into two U-shape measuring tubes. An excitation signal is emitted by the drive unit as a mechanical force on the U-shape tube, and the measuring tube vibrates continuously in the second-order vibration mode. Sensors A and B are used to detect the phase changes of the tube.

When the fluid flows in the pipe, the measuring tube is twisted due to Coriolis force. This causes the phase of the feedback signals of the detection sensor A and B to be ahead and lag behind the phase of the driving signal, respectively. The phase relationship between sensors A and B is shown in Figure 2.

A_0 represents the amplitude of the vibration signal of the drive unit, and A_1 and A_2 represent the amplitude of sensors A and B, respectively. According to the phase difference between sensors A and B, the mass flow rate of the CMF at this moment can be obtained as shown in the following formula:

$$q_m = \frac{K_s}{8r^2}\Delta t. \tag{1}$$

q_m is the mass flow rate, K_s is the angular elastic modulus of the measuring tube, r is the radius of the measuring tube, and Δt is the time difference between the two sides of the coil passing through the centerline.

2.2. CMF Wall-Mounted Failure Detection Method and Design. The sensors are divided into two groups. Array 1 consists of two external acceleration sensors distributed on the baffle plate in Figure 1(a); array 2 consists of the two sensors and drive unit as shown in Figure 1(a).

The specific anomaly detection progress is shown in Figure 3.

Step 1. After the array captures the vibration signal, the FastICA is used to decompose the signals of the two arrays to obtain the original signals.

Step 2. The wavelet scattering network is used to extract the features of the original signal, which is used to train the SVDD anomaly detection model.

Step 3. Finally, the single-classification algorithm based on SVDD is used to detect the CMF impurity adhesion. If the collected sensor array data is solved outside the hypersphere, it is believed that impurities are adhering to the pipe wall at this time.

Step 1. Fast independent component analysis.

The propagation path of waves in stainless steel is complex, and the propagation speed is fast. It is difficult to describe it with an accurate propagation model. In this paper, the simplified model is selected, and the linear hybrid FastICA is used to decompose the array signals. The FastICA aims to estimate the source signal S and the mixed matrix A by observing variable X.

There are three independent sound sources in Figure 4. A single microphone receives the mixed signals of the three

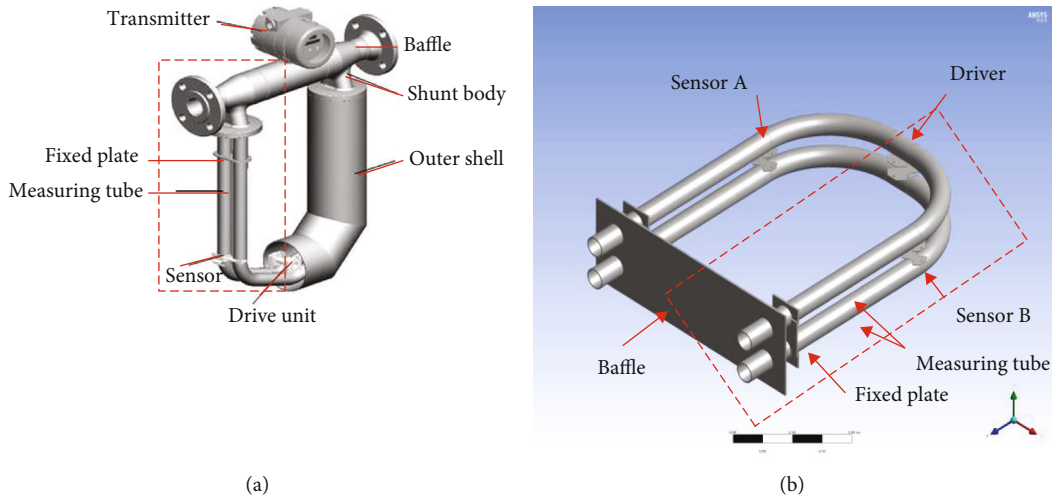

Figure 1: (a) The structure of CMF. (b) The primary instrument of CMF.

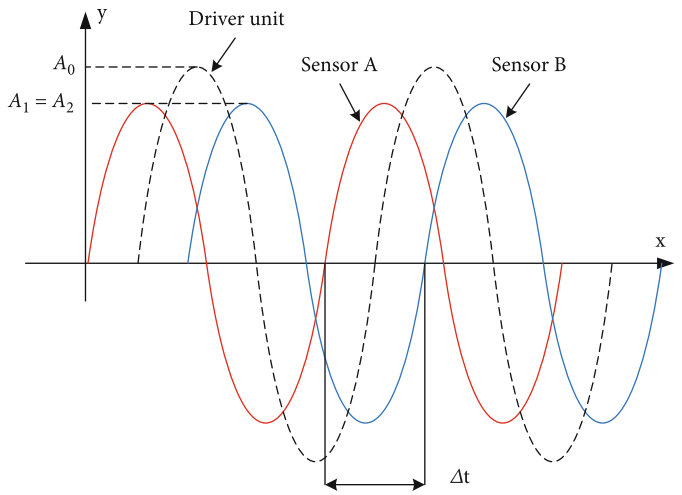

Figure 2: Drive unit, sensor A and B output signals.

sound sources. Due to the different distances between the sound source and each microphone, the wave signals received by each microphone are different.

There are n signal sources $(s_1, s_2, \cdots, s_n)$, S is an independent signal source, and A is an unknown mixed matrix, which is used to combine and construct observation variable X, which can be expressed as

$$X = AS. \tag{2}$$

Through the sensor array, the variables X can be obtained. According to the central limit theorem, the distribution of the combination of multiple random variables tends to Gaussian distribution. Finding an optimal direction W maximizes the non-Gaussian property of S in this direction. Thus, $\widehat{S} = W^T X$, negative entropy is used to measure non-Gaussianness:

$$J(s) = H\left(s_{\text{gauss}}\right) - H(s). \tag{3}$$

$H(*)$ is differential entropy, and s_{gauss} is a Gaussian random variable with the same covariance matrix as s. In a sense, negative entropy is the optimal estimation of non-Gaussian. Negative entropy is usually solved by the approximate method of negative entropy. One of the classical methods is the following equation [20]:

$$J(s) = \left[E\{G(s)\} - E\{G(v)\}\right]^2. \tag{4}$$

Type of $G(*)$ is a nonlinear function, and v is the standard normal distribution of random variables $E\{G(v)\}$ will be a constant. We only need to care about the value of $E\{G(W^T X)\}$. According to the Karush-Kuhn-Tucker condition, the optimal solution of equation (4) under the condition of $E\{(W^T X)^2\} = \|W\|_2 = 1$ can be expressed as the following equation:

$$\frac{\partial\left(J(s) - \beta\left(\|W\|^2 - 1\right)\right)}{\partial W} = E\left\{XG'\left(W^T X\right)\right\} - \beta W = 0. \tag{5}$$

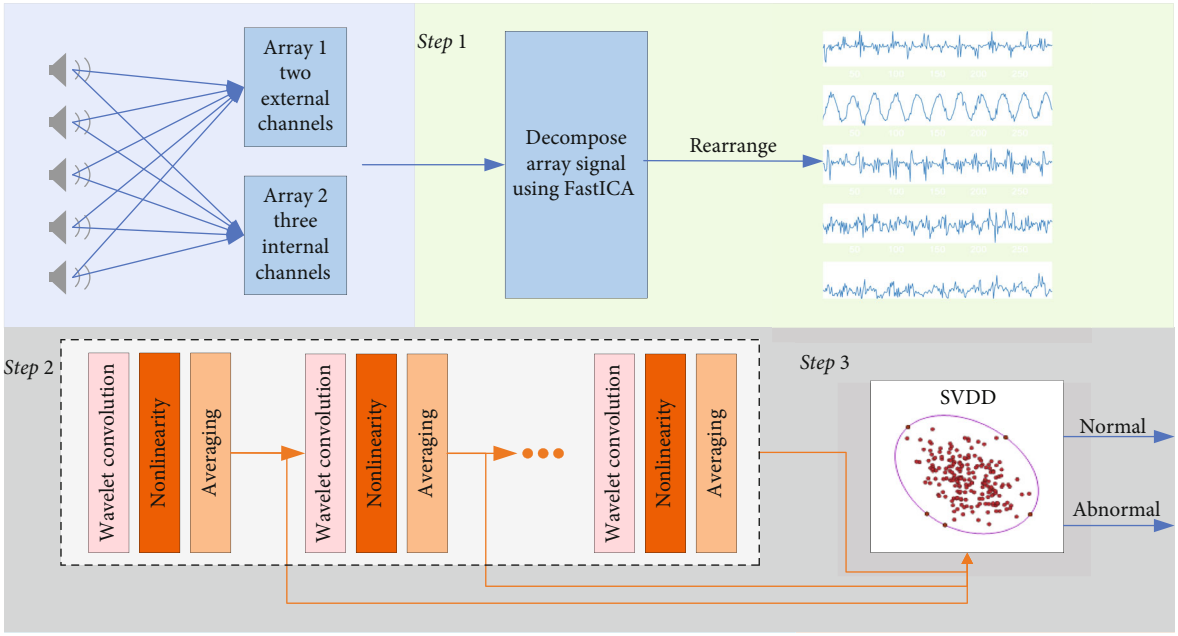

Figure 3: Anomaly detection progress.

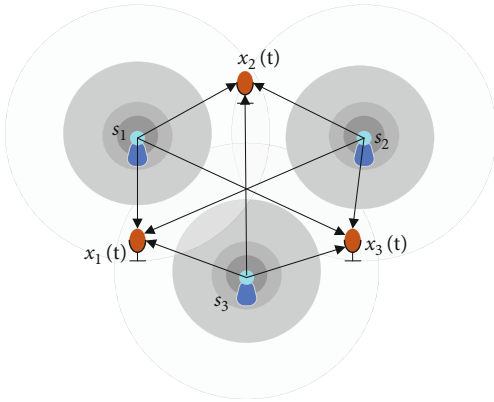

Figure 4: Blind source separation model.

The coefficient β is the Lagrange multiplier, and it is used to constrain the expectation of $E\{XG'(W^TX)\}$. Equation (5) can be expressed as follows:

$$W_{n+1} = W_n - \frac{E\left\{XG'\left(W_n^TX\right)\right\} + \beta W_n}{E\left\{XX^TG''\left(W_n^TX\right)\right\} + \beta}. \quad (6)$$

Under the condition of $E(XX^T) = I$, simplify equation (6), equation (7) is obtained.

$$W_{n+1} = E\left\{XG'\left(W_n^TX\right)\right\} - E\left\{G''\left(W_n^TX\right)\right\}W_n. \quad (7)$$

In this experiment, there is no requirement for amplitude, and the normalized processing of the obtained results can be obtained as follows:

$$W_{n+1} = \frac{W_{n+1}}{|W_{n+1}|}. \quad (8)$$

W is initialized as the identity matrix. Due to the uncertainty of the order of decomposition results of the FastICA, kurtosis is used as the sorting criterion to reorder the decomposed S to ensure that the array signal decomposition results are composed in a certain order and avoid the influence of order-disorder on feature extraction [21].

Step 2. Wavelet transform.

Various methods are used to generate signal features, such as the calculation of signal statistical characteristics and frequency-domain features [22]. The invariant scattering convolution network is used to automatically extract signal features with excellent performance and high interpretability. It contains wavelet convolution, nonlinear, and averaging operations [23, 24].

The complex wavelet transform for signal x is expressed as

$$x * \psi_{\lambda 1}(t) = x * \psi^a_{\lambda 1}(t) + jx * \psi^b_{\lambda 2}(t). \quad (9)$$

The extended wavelet $\psi_{a,b}(t)$ is obtained by the main wavelet $\psi(t)$ transform. The wavelet modulus coefficient is constructed by a complex wavelet and can be expressed as

$$U[\lambda]x = |x(t) * \psi_\lambda| = \sqrt{|x * \psi^a_{\lambda 1}(t)|^2 + |x * \psi^b_{\lambda 2}(t)|^2}. \quad (10)$$

The wavelet scattering coefficients with translation invariance can be obtained by convolving the modulus of

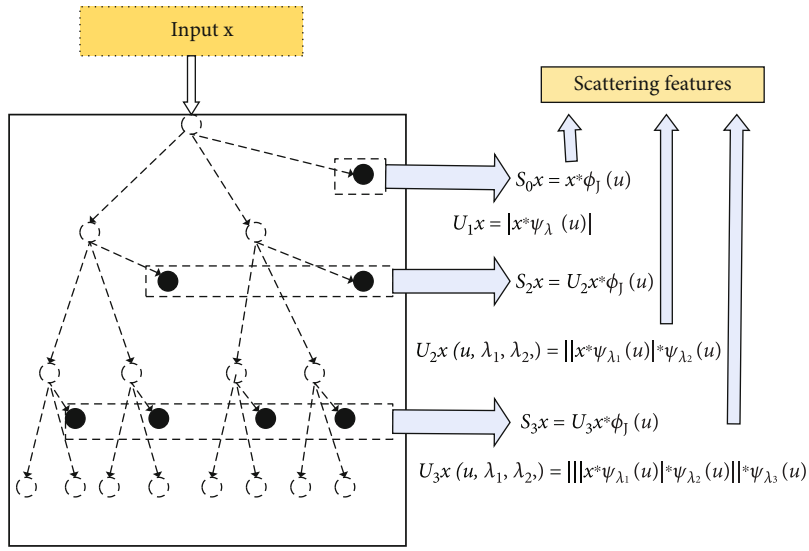

Figure 5: Invariant scattering convolution network.

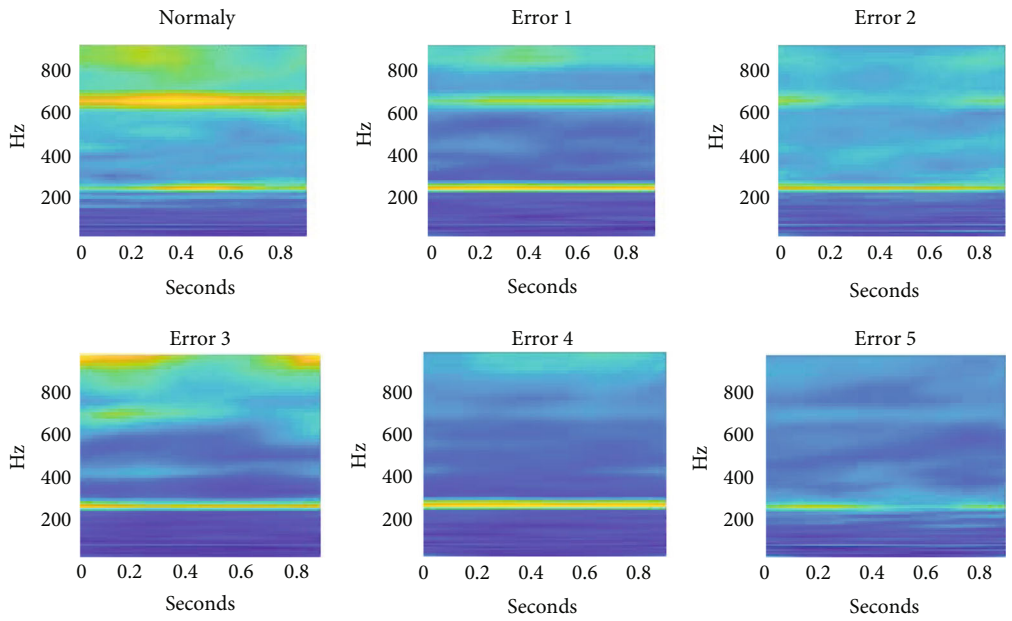

Figure 6: Wavelet scattering coefficient.

wavelet coefficients with the scaling coefficient function to obtain the low-frequency information of the signals:

$$[\lambda]x = |x(t) * \psi_\lambda| * \phi(t). \tag{11}$$

$\phi(t)$ is the scaling coefficient function of the low-pass filter.

The invariant scattering convolution network is shown in Figure 5. First, the signal is averaged using a wavelet low-pass filter, which loses the high-frequency details. A continuous wavelet transform is then applied to the signal to generate a set of diagrams of scale coefficients used to capture the details lost in the first step. After taking the modulus of scaling coefficients, the output is filtered using a wavelet low-pass filter to generate the first layer of scattering coefficients. In the end, repeat the process mentioned above to construct more layers of scattering coefficients.

Figure 6 shows the result of the signal of the two-channel accelerometer sensors after processing by FastICA placed on the fixed plate. For the six cases in the experiment, the scattering coefficients of the first decomposed component are very similar. Figure 6 shows the visualization of set 1 of the scattering coefficient filter for the second decomposed component. It can be seen from Figure 6 that there are significant differences in scattering characteristics between those with and without impurities adhered to the pipe wall.

An invariant scattering convolution network is a special kind of convolutional network. As the preset wavelet basis and nonlinear operators are set in advance, there is no need to adjust filter parameters through training samples, which

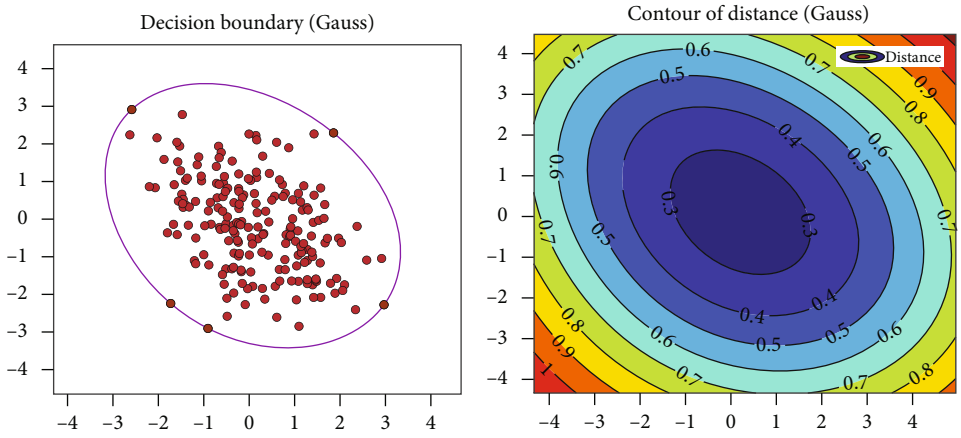

Figure 7: SVDD anomaly detection hypersphere.

greatly reduces the number of operations and computational complexity [25].

Step 3. Support vector data description.

In this paper, an attempt was made to hang impurities on the fixed points of the pipe wall to simulate the adhesion of impurities in the pipelines of CMF. Usually, the model can only be trained using data from the normal working state of CMF lacking counterexample data [26, 27]. This paper adopts a single classification algorithm based on SVDD to achieve the anomaly detection of impurity adhesion cases to solve this problem of extreme class imbalance [28, 29].

Tax and Tuin first proposed SVDD based on a support vector machine (SVM). This data description can be used for novelty or outlier detection. The primary detection principles are as follows.

Try to find a hypersphere with the smallest volume and wrap all the positive sample data in the hypersphere to complete the description of the target data region. Assuming that there is a class of positive sample data $x \in R^{n*d}$, where n is the number of samples and d is the feature dimension. The SVDD is used to find a hypersphere with the smallest volume which contains the positive class sample data, the center of the hypersphere is a, and the radius is R, which is transformed into the optimization problem:

$$\min R^2 + C\sum_{i=1}^{n}\xi_i, \tag{12}$$

$$\text{s.t.}\|x_i - a\|^2 \le R^2 + \xi_i, \xi_i \ge 0. \tag{13}$$

In equations (12) and (13), ξ is the slack variable, and C is the penalty coefficient. The introduction of slack variables allows some of the samples not to be in the hypersphere, which reduces the volume of the hypersphere and reduces the risk of overfitting.

As shown in Figure 7, if the image of the new sample point falls into the optimal hypersphere in the feature space, the sample is regarded as a normal point. Conversely, if the image of the new sample falls outside the optimal hypersphere in the feature space, the new sample is regarded as an outlier. In this way, the judgment of novelty or outlier detection is completed.

3. Simulations and Experiments

3.1. Modelling and Analysis. To carry out the research work and make the protocol feasible, the ANSYS simulation modelling shown in Figure 8(a) was completed to obtain the flow velocity distribution of the fluid within the CMF. According to the flow velocity distribution, the location of the CMF measuring tube that is most prone to wall-mounted failure is identified. The flow velocity of the measuring tube bend part of CMF is the greatest. When the flow body is viscous or contains impurities and flows through the bend pipe, it is not easy to appear viscous fluid or impurities deposition. At the location where the straight pipe intersects with the bend, the flow velocity of the fluid is the smallest, the probability of impurities hanging on the wall is the largest, and deposition is likely to occur.

Because the actual situation of the measuring tube impurity adhesion is complicated, the impurity adhesion's position and quality are difficult to accurately describe by the model, so this paper adopts a fixed-point wall-mounted study. Assuming that the density of impurities is greater than the density of the measured fluid, the location where the straight pipe intersects the bent pipe is taken as the location of impurity deposition. Blu-Tack is used to represent the impurities coated on the wall of the pipe to simulate the situation of impurities deposited and adhered in the measuring tube.

The Blu-Tack is pressed into a thin sheet and pasted on the pipe wall at the Figure 8(b) mark to simulate impurity deposition and adhesion to the pipe. The mass of plasticine pasted in a single position is 3 grams. There are a total of six conditions, respectively: (1) no impurity adhesion; (2) there is only one impurity adhesion; (3) there are two impurity adhesions on a measuring tube; (4) there is an impurity adhesion on each of the two measuring tubes; (5) there is one impurity adhesion on one measuring tube and two

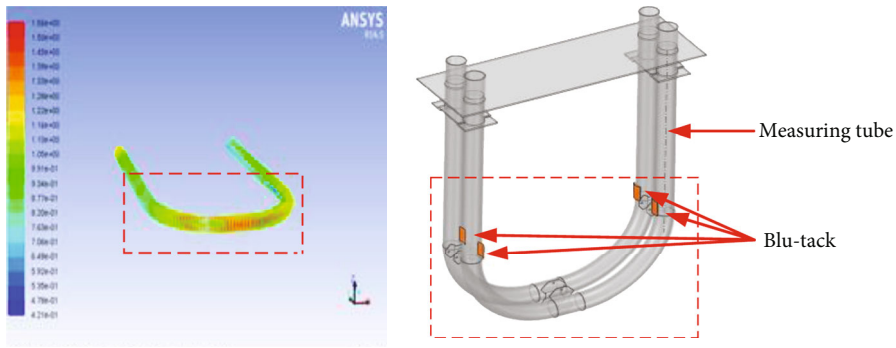

Figure 8: (a) CMF velocity simulation. (b) Experimental model of the CMF.

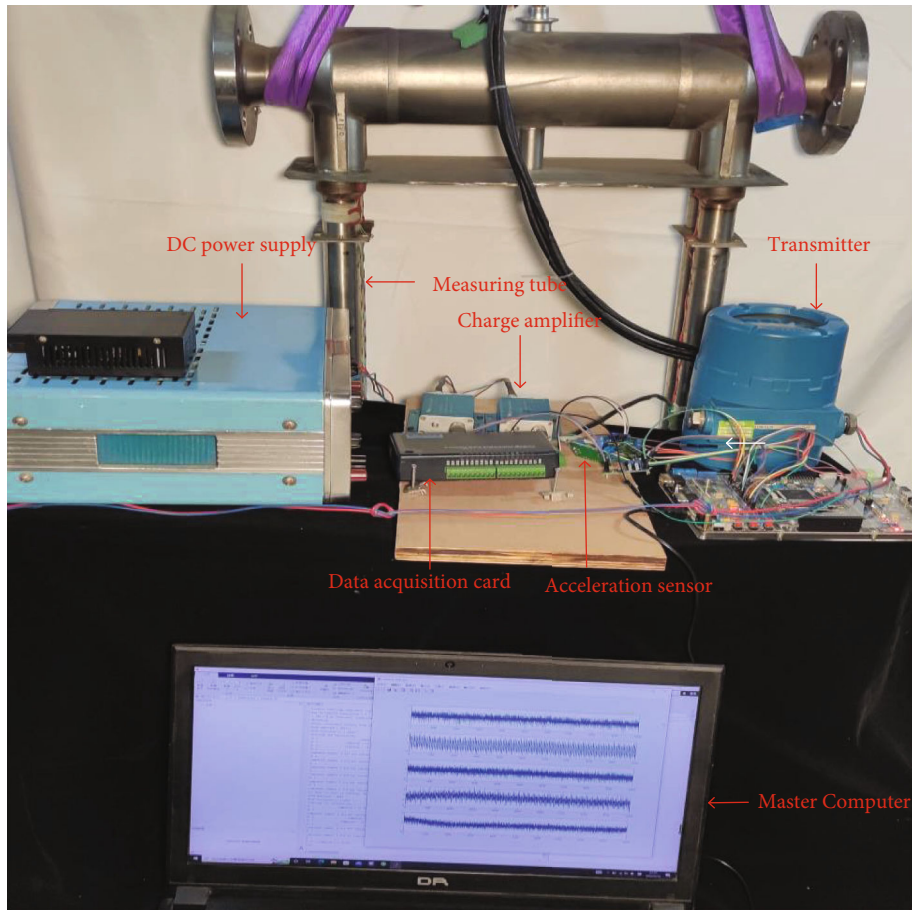

Figure 9: Experimental site device diagram.

impurities adhesion on the other measuring tube; (6) there are two impurity adhesions on both measuring tubes.

3.2. Experimental Platform and Setups. In this experiment, the required equipment includes N50 double U-shaped CMF and N50 double U-shaped CMF sensor matching DPT100 transmitter, Blu-Tack (used to simulate impurities), resolution of 0.01 electronic balance (weighing Blu-Tack), acceleration sensor of LC0403 vibration sensor, BVM-8101 microcharge amplifier, DC voltage regulator power supply, data acquisition card USB-4716, and a master computer. The on-site device is shown in Figure 9.

A total of 30,000 sets of data were collected in this paper, including 20,000 sets of CMF normal operation data and 2000 sets of data of five wall-mounted experimental arrays, each with a length of 1 second. The contamination parameter is set to 0.1, indicating the proportion of contaminated data in the positive sample data set.

In the experiment, the sensor data of CMF under normal working conditions are collected first. Then, the FastICA is

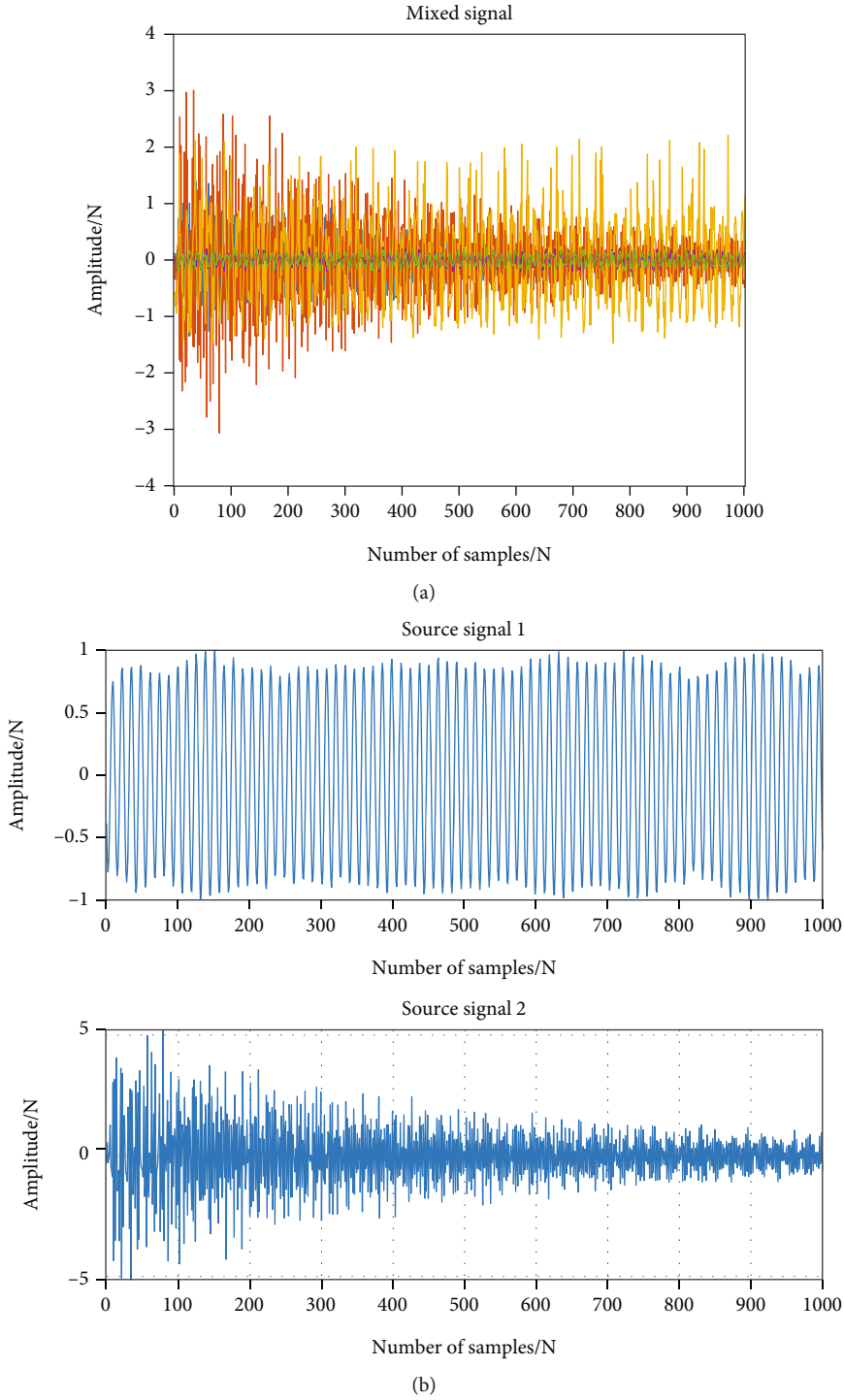

Figure 10: (a) Vibration signal of CMF. (b) FastICA decomposition results.

used to decompose the signal array, and the wavelet scattering features are extracted and selected. Finally, the detection model of SVDD is trained to obtain the spherical center and the decision boundary. If the collected sensor array data is outside the hypersphere after calculation, it can be considered that impurities are adhering to the pipe wall in CMF at this moment. On the contrary, it is considered that no impurities are adhering to the pipe wall in CMF at this moment. Reasonable explanations of simulation results and experimental data are given at the end.

3.3. Percussion Experiment of CMF. The validity of the theory requires specific experiments to verify. Therefore, this percussion experiment is used to verify the effectiveness of the FastICA algorithm in CMF array signal decomposition. When CMF is in a normal working state, a slight percussion

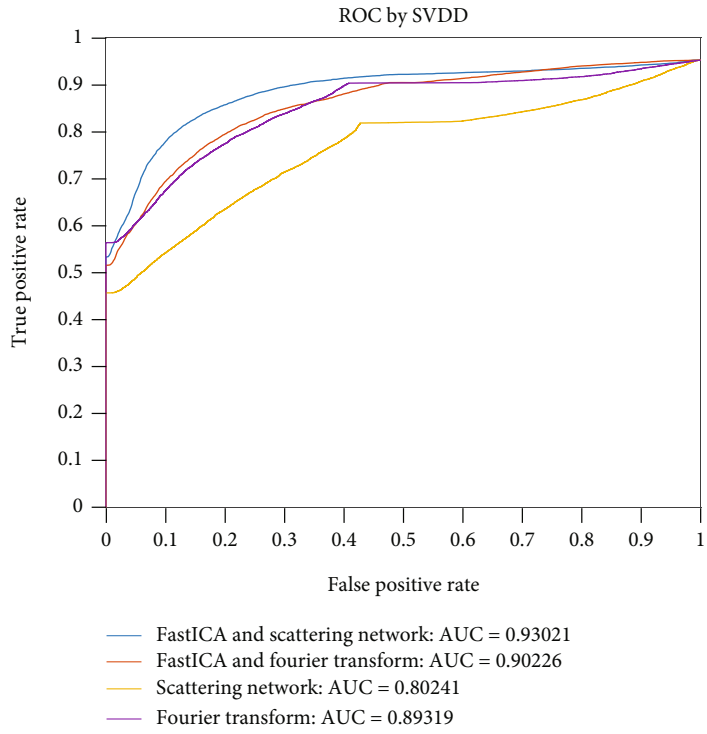

Figure 11: ROC curve of CMF fault detection.

Table 1: Confusion matrix.

	Predicted normally	Predicted anomaly
Actual normally	18000	2000
Actual anomaly	1124	8876

is given to the measuring tube, and the vibration signal of CMF is collected through the vibration data acquisition experimental platform.

The array signal of CMF is shown in Figure 10, where the x-axis is the number of sampling points while the y -axis is the amplitude. The CMF vibration signal waveform plot is shown in Figure 10(a), and the components obtained by FastICA decomposition are as shown in Figure 10(b). It can be concluded that source signal 1 is the signal transmitted to the outer shell by the vibration of the measuring tube during the normal operation of the CMF. Source signal 2 is the percussion signal to the measuring tube. The FastICA algorithm can effectively separate the mixed signals of CMF array signals through the analysis of experimental results.

3.4. Results and Discussion. The invariant convolution scattering networks and Fourier transform are used to extract features of the signal. Only the normal working data of CMF are used to train the anomaly detection model proposed in this paper. It can be divided into four cases according to whether to use the FastICA algorithm to decompose the array signal and whether to use the invariant convolutional scattering network or the Fourier transform to extract the signal features. The receiver operating characteristic (ROC) curve is shown in Figure 11.

From the ROC curve, the FastICA algorithm to decompose the signal can improve the performance of the anomaly detection algorithm. The area under curve (AUC) metric significantly improved from 0.89319 to 0.93021 in the case of decomposing the signal by using the FastICA algorithm and extracting features by using an invariant convolutional scattering network. In this paper, the signal features extracted using the invariant convolutional scattering network are more efficient than the Fourier transform.

For the experiments, the array signal was processed using the anomaly detection algorithm in Figure 3, and the confusion matrix is shown in Table 1.

Even if few impurities adhere to the tube wall, the method could still be effectively monitored, and decent results can be achieved. Although the difference of the small additional mass reflected in the signal is very weak, the method proposed in this paper can reach the detection accuracy of 89.59%.

4. Conclusions

In this paper, the finite element analysis model of CMF is established based on the ANSYS Workbench platform, and a CMF wall-hanging fault detection algorithm based on an array sensor is proposed. 5 g plasticine is used to simulate impurities for experiments. Some conclusions can be derived according to the series of simulations and practical experiments.

(1) *Fault Location Prediction*. The location most prone to wall-mounted failure is obtained by simulation, which is regarded as the location of the wall-mounted failure to establish the model

(2) *Fault Detection Algorithm*. The wall-hanging fault detection algorithm of CMF based on an array sensor is proposed, and 5 g plasticine is used to simulate impurities for experiments. Finally, the accuracy of experimental results can reach 89.59%

(3) *Application Advantages*. The algorithm proposed in this paper can detect whether there are impurities attached to the CMF wall in real-time. The detection effect is good, which further ensures the long-term efficient operation of CMF and reduces the cost of enterprises. At the same time, this method can be widely used in ultrasonic array detection signal processing, pattern recognition, anomaly detection, and data classification

Data Availability

The data used to support the findings of this study are available from the corresponding author upon request.

Conflicts of Interest

The authors declare that they have no conflicts of interest.

Acknowledgments

This work was supported in part by the Key R & D Program of Shaanxi Province under Grant D5140190030 and in part by the National Natural Science Foundation of China under Grant 51875477.

References

[1] P. Zhang, M. C. Kang, and B. Wang, "The influencing factors on the vibrating tubes abrasion of Coriolis mass flowmeter," *Industrial instrumentation and automation equipment*, vol. 3, pp. 91–94, 2011.

[2] J. X. Ren, Q. Sun, and P. Zhang, "Research on measurement technique of fluid viscosity and realization with ZLJC mass flowmeter," *Instrument Technique and Sensor*, vol. 10, pp. 31–34, 2013.

[3] K. J. Xu, *Flow Sensor Signal Modeling, Processing and Implementation*, Science Press, 2011.

[4] S. Q. Cao, H. T. Zhang, and Y. Q. Tu, "On-line detection method based on resonant frequency for dirt in U-shaped tube Coriolis mass flowmeter," *Instrument Technique Sensor*, vol. 6, pp. 30–33, 2017.

[5] Y. T. Gao, M. Zhang, and J. X. Ren, "Analysis of Coriolis mass flowmeter life based on ANSYS," *Mechatronics*, vol. 20, no. 2, pp. 42–81, 2014.

[6] C. Tan, X. Li, H. Liu, F. Dong, and F. Dong, "An ultrasonic transmission/reflection tomography system for industrial multiphase flow imaging," *IEEE Transactions on Industrial Electronics*, vol. 66, no. 12, pp. 9539–9548, 2019.

[7] U. Ewert, "Current Trends in Digital Industrial Radiography - from Nano to Macro Scale," *2017 Far East NDT New Technology & Application Forum (FENDT)*, pp. 312–317, 2017.

[8] C. P. Stark, A. T. Patten, M. A. Butler, and G. R. Duffel, *Diagnostic Equipment and Method for Coriolis Flowmeter*, CN101334305, USA, 2008.

[9] J. Yang, M. Chen, and L. X. Zhang, "Fault detection and correction algorithm of section mass flowmeter," *Sensors and Microsystems*, vol. 23, no. 2, pp. 56–58, 2004.

[10] Y. P. Gao, J. Yang, and M. Chen, "Study on fault detection and correction of Coriolis mass flowmeter," *Sensors and Microsystems*, 2005.

[11] C. Sun and X. Q. Wang, "On-line and off-line verification of mass flowmeter," *Northwestern Industrial metrology*, vol. 17, no. 4, pp. 27–30, 2004.

[12] M. G. Wheeler, D. F. Knowlman, M. J. Bell, and M. T. Crisfield, *Diagnostic Device and Method for Coriolis Flowmeter*, CN1860350, USA, 2006.

[13] L. W. Wang, X. C. Luan, Y. D. Shua, and L. Yuan, "Fault extraction of roller bearing outer ring scratch in the complex path based on fast ICA," *Machinery Design and Manufacture*, vol. 12, pp. 77–81+87, 2021.

[14] A. Hyvärinen, E. Oja, and E. Oja, "Independent component analysis: algorithms and applications," *Neural Networks*, vol. 13, no. 4-5, pp. 411–430, 2000.

[15] Y. Yuan, W. Jiawen, Z. Desheng, W. Jiachen, W. Tonghai, and Y. Kehu, "Feature extraction and classification method of coal gangue acoustic signal during top coal caving," *Journal of Mining Science and Technology*, vol. 6, no. 6, pp. 711–720, 2021.

[16] Y. Hu, X. T. Yuan, L. Y. Chen, Z. H. Jiang, and W. Liu, "GNSS-IR sea surface height inversion model based on wavelet transform and improved burg algorithm," *Geodesy and geodynamics*, vol. 42, no. 1, pp. 21–24+53, 2022.

[17] T. Wang, M. C. Zhang, Q. H. Yu, and H. Y. Zhang, "Comparing the applications of EMD and EEMD on time-frequency analysis of the seismic signal," *IEEE Journal of Selected Topics in Applied Earth Observations and Remote Sensing*, p. 99, 2021.

[18] M. Sifuzzaman, "Application of wavelet transform and its advantages compared to Fourier transform," *Journal of Physical Sciences*, 2009.

[19] J. Xu, J. Yao, and L. Ni, "Fault detection based on SVDD and cluster algorithm," in *2011 International Conference on Electronics," 2011 International Conference on Electronics, Communications and Control (ICECC)*, pp. 2050–2052, Ningbo, China, 2011.

[20] C. Ji, Y. Yu, and P. Yu, "A new FastICA algorithm of Newton's iteration," in *2010 2nd International Conference on Education Technology and Computer*, p. V3-481, Shanghai, 2010.

[21] M. Bressan, D. Guillamet, and J. Vitria, "Using an ICA representation of high dimensional data for object recognition and classification," in *Proceedings of the 2001 IEEE computer society conference on computer vision and pattern recognition, pp. I-I*, Kauai, HI, USA, 2001.

[22] A. Hyvärinen and E. Oja, "A fast fixed-point algorithm for independent component analysis," *Neural Computation*, vol. 9, no. 7, pp. 1483–1492, 1997.

[23] J. Andén and S. Mallat, "Deep scattering spectrum," *IEEE Transactions on Signal Processing*, vol. 62, no. 16, pp. 4114–4128, 2014.

[24] S. Mallat, "Understanding deep convolutional networks," *Philos Trans A Math Phys Eng*, vol. 374, p. 2065, 2016.

[25] J. Bruna and S. Mallat, "Invariant scattering convolution networks," *IEEE Transactions on Pattern Analysis and Machine Intelligence*, vol. 35, no. 8, pp. 1872–1886, 2013.

[26] F. Rashid and A. Miri, "User and event behavior analytics on differentially private data for anomaly detection," in *2021 7th IEEE Intl Conference on Big Data Security on Cloud (Big Data Security), IEEE Intl Conference on High Performance and Smart Computing (HPSC) and IEEE Intl Conference on Intelligent Data and Security (IDS)*, pp. 81–86, NY, USA, 2021.

[27] S. Katsumata, D. Kanemoto, and M. Ohki, "Applying outlier detection and independent component analysis for compressed sensing EEG measurement framework," *Biomedical Circuits and Systems Conference (BioCAS)*, pp. 1–4, 2019.

[28] D. M. J. Tax, R. P. W. Duin, and R. P. W. Duin, "Support vector domain description," *Pattern Recognition Letters*, vol. 20, no. 11-13, pp. 1191–1199, 1999.

[29] M. Yao and H. Wang, "One-Class Support Vector Machine for Functional Data Novelty Detection," *2012Third Global Congress on Intelligent Systems*, pp. 172–175, 2012.